Macromolecules

Article

pubs.acs.org/Macromolecules

# Functional Supramolecular Polypeptides Involving $\pi-\pi$ Stacking and Strong Hydrogen-Bonding Interactions: A Conformation Study toward Carbon Nanotubes (CNTs) Dispersion

Cheng-Wei Huang,[†] Mohamed Gamal Mohamed,[‡] Chao-Yuan Zhu,[†] and Shiao-Wei Kuo*[,‡]

[†]Institute of Applied Chemistry, National Chiao Tung University, Hsinchu 300, Taiwan

[‡]Department of Materials and Optoelectronic Science, National Sun Yat-Sen University, Kaohsiung 804, Taiwan

Supporting Information

**ABSTRACT:** New supramolecular polypeptides have been prepared through simple ring-opening polymerization and "click" reactions. Postfunctionalization with diaminopyridine (DAP) moieties, capable of multiple hydrogen bonding, was an efficient approach toward forming $\alpha$-helical-dominant polypeptides. The physically cross-linked networks produced upon self-organization of the DAP units increased the glass transition temperature ($T_g$) of the polymers and sustained the secondary structures of the polypeptides. Additional thermal responsivity resulted from dynamic noncovalent bonding on the polymer side chains. Molecular recognition through heterocomplementary DAP···thymine (T) base pairs was revealed spectroscopically and then used to construct poly($\gamma$-propargyl-L-glutamate)-*g*-*N*-(6-acetamidopyridin-2-yl)-11-undecanamide/thyminylpyrene (PPLG-DAP/Py-T) supramolecular complexes. Transmission electron microscopy images revealed that this complex was an efficient dispersant of carbon nanotubes (CNTs). Indeed, it could disperse CNTs in both polar and nonpolar media, the direct result of combining two modes of secondary noncovalent bonding: multiple hydrogen bonding and $\pi-\pi$ interactions. Furthermore, CNT composites fabricated with biocompatible polymers and high value of $T_g$ should enable the development of bio-inspired carbon nanostructures and lead the way toward their biomedical applications.

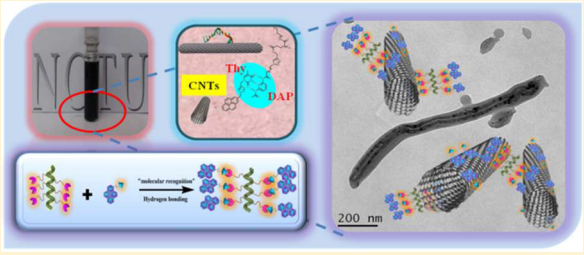


## INTRODUCTION

Self-assembly phenomena occur ubiquitously in nature and in our daily lives.[1] In addition, self-assembly has been incorporated in the design a variety of new functional materials, extending the range of interesting structures beyond the molecular level.[2] Although the self-assembly of molecules into one-dimensional multicomponent structures has been known for decades, only recently have supramolecular polymers attracted steadily increasing interest due to their unprecedented and highly useful properties.[3] Among these supramolecular polymers, polypeptides are particularly fascinating materials because of their potential application in nanochemistry and biomimetics (e.g., bioelectronics,[4] drug carriers,[5] tissue engineering[6]). The protein-like structures of polypeptides, which provide a link between chemistry and biology, can be prepared under mild conditions with relatively simple functionalization processes.[7] In addition, synthetic polypeptides can form unique hierarchically ordered structures: for example, rigid-rod-like $\alpha$-helices dominated by intramolecular hydrogen-bonding interactions or $\beta$-sheet conformations stabilized through intermolecular hydrogen bonding. New properties can also result when helical polypeptides are conjugated with other functional units.[8] As a result, the continued design of novel supramolecular architectures can lead to several prospective applications.

As a result of their extended $\pi$-electron systems and unique one-dimensional structures, carbon nanotubes (CNTs) have excellent optoelectronic, mechanical, and thermal properties.[9] In addition, their behavior can be highly responsive to their chemical or physical environment.[10] These phenomena can be used to fabricate nanoscale sensors that take advantage of photoluminescence (PL) quenching effects arising from molecular adsorption events on CNT surfaces.[11] Attempts to make practical use of these properties have been hampered, however, by the surfaces of CNTs being highly polarizable with large attractive intertubular van der Waals forces, leading to the formation of extremely hydrophobic and insoluble aggregates that greatly hinder their assemble into useful structures.[12] Substantial efforts have been exerted to develop strategies to debundle or disperse CNTs. For example, covalent attachment of polar groups or simple oxidation of CNTs can lead to slight improvements in their dispersibility in organic solvents. Covalent surface modification with polypeptides using the "graft-from" approach[13] and the application of CNT initiators for polymer synthesis[14] have also been proposed. Nevertheless, the resulting changes in the $sp^2$-to-$sp^3$ ratio can negatively affect

**Received:** May 19, 2016
**Revised:** July 9, 2016
**Published:** July 22, 2016

Downloaded via NATL SUN YAT-SEN UNIV on April 24, 2020 at 09:06:53 (UTC).
See https://pubs.acs.org/sharingguidelines for options on how to legitimately share published articles.

ACS Publications © 2016 American Chemical Society



DOI: 10.1021/acs.macromol.6b01060
*Macromolecules* 2016, 49, 5374−5385

the inherent properties of CNTs.[15] Recently, attention has been focused on strategies that preserve the entire $\pi$-network of the CNTs. Indeed, dispersant-assisted dispersion has been used widely to achieve nondestructive dispersion,[16] with small molecule-based surfactants, conjugated polymers, and other biomaterials often chosen as the dispersants.[17] Polypeptides that form $\alpha$-helical secondary structures are newly arising materials for use as dispersants. These bio-inspired folded springlike architectures with side chain units extending outside the helix can function as surfactants that minimize the surface energy of the entire system. Selective binding or adsorption of polypeptides to various materials (metals, metal oxides, semiconductors) has been exploited.[13,18] The ability to inspect the structures formed from CNT/polypeptide composites and to facilitate the dispersion of CNTs with designed peptides should benefit further biomedical and biophysical applications of these materials.

Synthetic polymers receive much attention because their useful properties can be exploited for technological advancement. Nevertheless, these materials are composed mainly of irreversible covalent bonds, which limit the range of structures and functions that can be accessed by the polymer matrix. In contrast, supramolecular polymers enable the direct association of discrete building blocks into versatile coiled chains or highly ordered frameworks.[19] The constituents of these materials are bridged through dynamic noncovalent linkages (e.g., electrostatic interactions, hydrogen bonding) that simultaneously provide additional recyclability, applications in stimuli detection,[20] and inherently defect-free architectures.[21] Highly directional interactions—for example, multiple hydrogen bonding—can be powerful tools because of their strength and versatility, when preparing monocomponent assemblies.[22] Although hydrogen-bonded assemblies can have many attractive features, fewer reports have appeared describing the applications of multicomponent supramolecular complexes. In a previous study, we developed a supramolecular complex system for the dispersion of a crystalline dye.[23] As reported, supramolecular polymers may have the ability to wrap around the graphitic side walls of CNTs.[21] To the best of our knowledge, however, very few papers have appeared describing hydrogen-bonded supramolecular polymers as dispersing agents, especially for use as biomaterials. Herein, we discuss the preparation and application of a supramolecular functioned polypeptide prepared through ring-opening polymerization (ROP) of a glutamate *N*-carboxyanhydride (NCA) using an alkylamine as the initiator and postfunctionalization with diaminopyridine (DAP)—a donor−acceptor−donor (DAD) multiple hydrogen-bonding unit—through copper(I)-catalyzed alkyne/azide cycloaddition (CuAAC). The polymeric products were characterized using nuclear magnetic resonance (NMR) spectroscopy, Fourier transform infrared (FTIR) spectroscopy, and matrix-assisted laser desorption/ionization time-of-flight (MALDI-TOF) mass spectrometry. A study of the conformations of these polypeptides was then performed, with spectroscopic discussion, to investigate the interplay between the multiple hydrogen-bonding moieties and the polymer backbone. The complementary DNA nucleobase thymine (T) was then introduced to interact with the pyrene units to form another type of supramolecular guest structure capable of interacting with CNT surfaces. The specific strong hydrogen bonding of this base pair (DAP···T) led to the formation of supramolecular complexes containing dynamic noncovalent linkages. Exploiting these systems, CNT dispersion was examined in both polar and nonpolar media. A peptide/CNT composite prepared through solvent removal *in vacuo* displayed a high glass transition temperature ($T_g$), providing evidence for molecular recognition of its component species.

## EXPERIMENTAL SECTION

**Materials.** THF was refluxed with sodium prior to use. All solvents were purchased from TEDIA (USA) and distilled over $CaH_2$ before use. Copper(I) bromide (CuBr) was purified with glacial acetic acid and washed with absolute ethyl ether. Other commercially available reagents were obtained from Sigma-Aldrich, Acros, and Alfa Aesar were used as received. Az-acid, Az-DAP, and Ac-DAP were synthesized as mentioned in the Supporting Information and characterized as shown in Figures S1 and S2. $\gamma$-Propargyl-$_L$-glutamate *N*-carboxyanhydride, propargylthymine (PT), and Py-$N_3$ were prepared follow our previous report.[24] SWCNTs (main range of diameter: <2 nm; length: 5−15 $\mu$m) and MWCNTs (main range of diameter: 40−60 nm; length: 5−15 $\mu$m) were purchased from Centron Biochemistry Technology, Taiwan. SWCNTs and MWCNTs were purified with following method: CNTs were washed with toluene by sonication (4 h), ultrafiltrated, and then dried under vacuum to obtain the purified CNTs.

**Characterization.** $^1$H and $^{13}$C NMR spectra (and variable-temperature NMR spectra) were recorded from samples in $CDCl_3$, DMSO-$d_6$, or DMF-$d_7$ using an Agilent VMRS-600 NMR spectrometer operated at 600 and 150 MHz, respectively. The polydispersity index (PDI) and molecular weight information were calculated using a Waters 510 gel permeation chromatography (GPC) system (with three Ultrastyragel columns: 100, 500, and 1000 Å connected in series); dimethylformamide (DMF) was used as the eluent at 50 °C (flow rate: 0.8 mL min$^{-1}$). The calibration curve of the system was constructed with Agilent EasiCal polystyrene (PS) standards. Measurement was performed using a refractive index detector. MALDI-TOF mass spectra were measured using a BrukerDaltonicsAutoflex III spectrometer operated with the following parameters: ion source 1, 19.06 kV; ion source 2, 16.61 kV; lens, 8.78 kV; reflector 1, 21.08 kV; reflector 2, 9.73 kV. FTIR spectra were obtained using a Bruker Tensor 27 FTIR spectrometer. Samples were prepared with the KBr disk method and measured 32 scans with resolution of 1 cm$^{-1}$ at room temperature. The thermal stabilities were measured using a TA Q-50 thermogravimetric analyzer under a nitrogen atmosphere; the sample was first loaded in a Pt cell and then heated from 30 to 800 °C (rate: 20 °C min$^{-1}$) under a 60 mL min$^{-1}$ nitrogen flow. A Q-20 apparatus (TA) was chosen for differential scanning calorimetry (DSC) measurement under the atmosphere of dry $N_2$. Samples (3−5 mg) were scanned from −80 to 150 °C (rate: 10 °C min$^{-1}$) in a sealed aluminum pan. PL emission spectra were obtained in solution at 25 °C using a Hitachi F-4500 fluorescence spectrometer equipped with a monochromatized Xe light source. A JEOL-2100 TEM operated at an accelerating voltage of 200 kV was used to record transmission electron microscopy (TEM) images for further characterization.

**Preparation of Supramolecular Complexes.** Mixtures of PPLG-DAP and Py-T were prepared through solution blending. A DMF or 1,1,2,2-tetrachloroethane (TCE) solution containing 5 wt % of the polymer mixture was stirred for 12 h; the solution was then tested for CNT dispersion, or the solvent was evaporated slowly at room temperature for further characterization.

**CNT Dispersion in the Presence of Supramolecular Complexes.** Purified CNTs were dispersed with sonication in DMF or TCE for 2 h. A solution of the PPLG-DAP/Py-T supramolecular complex (prepared as described above) was then added dropwise into the CNT dispersion, followed by stirring at room temperature for 24 h. The precipitate was removed through three centrifugation/washing cycles, and then the supernatant of the CNT supramolecular dispersion was subjected to ultrafiltration through PALL membrane disc filters (FP-450 PVDF filter for DMF dispersion; ULTIPOR N66 nylon filter for TCE dispersion) to recover the supramolecular peptide/CNT composites. The composites (black powders) could be


DOI: 10.1021/acs.macromol.6b01060
*Macromolecules* 2016, 49, 5374−5385

Scheme 1. Synthesis of (a) PPLG-DAP and (b) Py-T; (c) Supramolecular Complex Formation

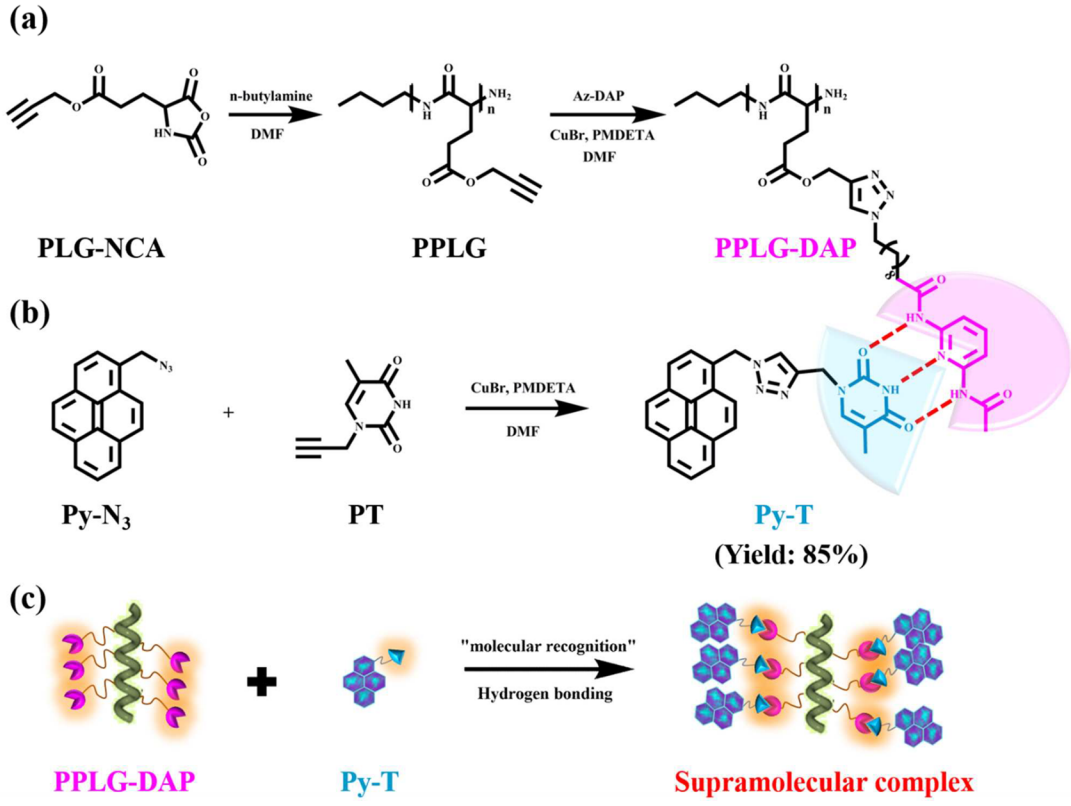


redispersed within 1 min after adding an organic solvent and sonicating in an ultrasonication bath.

## RESULTS AND DISCUSSION

**Synthesis of DAP-Functionalized Polypeptides.** The supramolecular peptide PPLG-DAP was prepared through a sequence of polymerization and "click" reactions (Scheme 1). First, a "click"-active propargyl group was introduced onto L-glutamic acid to form γ-propargyl-L-glutamate. A facile cyclization reaction with triphosgene yielded γ-propargyl-L-glutamate *N*-carboxyanhydride (PLG-NCA).[25] Amine-mediated ROP was then performed to provide the side-chain-graftable polypeptides PPLG. High-molecular-weight [$PPLG_{30}$; degree of polymerization (DP): 30] and low-molecular-weight ($PPLG_{10}$; DP, 10) polypeptides were synthesized for comparison. Characteristic peaks in the terminal alkyne (−C≡C stretching, 2129 $cm^{-1}$) and peptide amide regions appeared in the FTIR spectra (Figure 1c). After polymerization from PLG-NCA, a new absorbance at 3298 $cm^{-1}$ (N−H stretching) was observed. In addition, 1655 $cm^{-1}$, 1627 $cm^{-1}$ (amide I), and 1546 $cm^{-1}$ (amide II) appeared for PPLG and were attributed to amide bending vibration in peptide backbone. Ester C═O stretching occurs at 1742 $cm^{-1}$ for both $PPLG_{30}$ and $PPLG_{30}$DAP, therefore suggesting the alkyne functionality has been successfully introduced into side chain of polypeptides. The multiple hydrogen-bonding DAP functionality was then introduced through CuAAC with Az-DAP. $^1$H NMR and FTIR spectra were used to monitor the reaction progress. The signals for terminal alkyne stretching (2129 $cm^{-1}$) of PPLG and azide stretching (2092 $cm^{-1}$) of Az-DAP were both absent in the FTIR spectra of to the PPLG-DAP products (Figure 1). A change in chemical environment was also evidenced in the $^1$H NMR spectra (Figure 2). The signal of

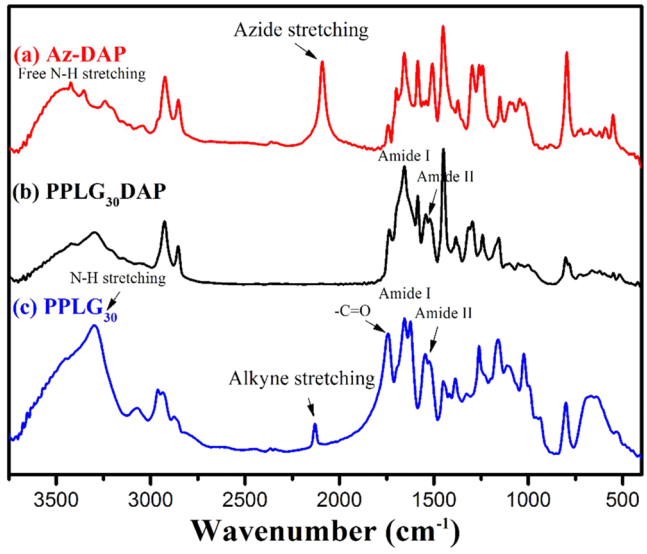


**Figure 1.** FTIR spectra of (a) Az-DAP, (b) $PPLG_{30}$DAP, and (c) $PPLG_{30}$.

the $CH_2N_3$ unit of Az-DAP appeared at 3.24 ppm; the signals of the alkyne proton and the propargylic $CH_2$ group appeared at 4.79 and 3.39 ppm, respectively, in the spectrum of PPLG. After the click reaction had formed PPLG-DAP, the signals for the azide and alkyne disappeared, while signals appeared at 5.20 and 4.39 ppm for the two types of $CH_2$ groups neighboring the newly formed triazole ring (7.72 ppm). Similar phenomena were evident in the corresponding $^{13}$C NMR spectra (Figure S3). The intensities of the characteristic peaks for the azide and propargyl groups finally disappeared completely at the



DOI: 10.1021/acs.macromol.6b01060
*Macromolecules* 2016, 49, 5374−5385

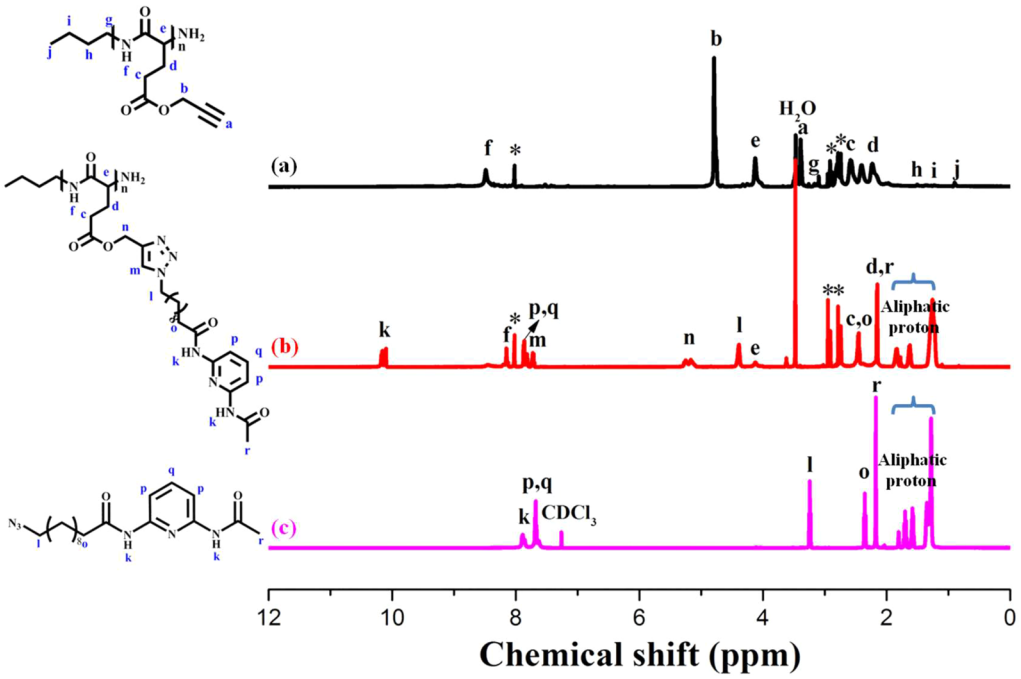


**Figure 2.** $^1$H NMR spectra of (a) $PPLG_{30}$, (b) $PPLG_{30}DAP$ in DMF-$d_7$, and (c) Az-DAP in $CDCl_3$ (asterisk represents residual DMF).

completion of the reaction in the corresponding FTIR spectra (Figure 1). The combined spectral data indicated that the high selectivity and specificity of the copper(I)-mediated click reaction were an efficient protocol for postfunctionalization of the polypeptide.

The molecular weights of the PPLG polymers with different DPs ($PPLG_{10}$, $PPLG_{30}$) and their postfunctionalized products ($PPLG_{10}DAP$, $PPLG_{30}DAP$) were calculated using various means. The DPs of the PPLGs, determined from $^1$H NMR spectra, are listed in Table 1. GPC with DMF as eluent was applied to investigate the change in molecular weight before and after postfunctionalization with DAP moieties. The retention times decreased after the "click" reactions of $PPLG_{10}$ forming $PPLG_{10}DAP$ (Figure 3a) and of $PPLG_{30}$ forming $PPLG_{30}DAP$ (Figure 3b), suggesting an increase in molecular weight as a result of side-chain grafting of each repeat unit. A similar trend was evident in the MALDI-TOF mass spectra (Figures 3c and 3d). The MALDI-TOF mass spectra of the polypeptides in Figure 3c feature distributions of $m/z$ values that are typical of polydisperse polymeric samples.[26] Each adjacent signal of $PPLG_{10}$ was separated by 167 Da, the molecular weight of a PLG repeat unit. After postfunctionalization, the interval between adjacent signals of $PPLG_{10}DAP$ was 527 Da, with the peak maxima of the spectra having shifted to higher molecular weight as a result of the change in the repeat unit's structure. The molecular weights calculated from the MALDI-TOF mass spectra were accord with those from the $^1$H NMR spectra, but lower than those measured using GPC because of different hydrodynamic radii in the DMF used as the eluent and the systematic deviation in the structures of the polypeptides and the standard PS used to obtain the GPC calibration curve.[24,27]

**Table 1. Characterization Data for the Polypeptides Used in This Study**

| polypeptides | $M_n$[a] | PDI[a] | $M_n$[b] |
|---|---|---|---|
| $PPLG_{10}$ | 3473 | 1.18 | 1759 |
| $PPLG_{30}$ | 12055 | 1.25 | 5133 |
| $PPLG_{10}DAP$ | 7130 | 1.24 | 4561 |
| $PPLG_{30}DAP$ | 30491 | 1.23 | 16044 |

[a]Calculated by GPC (DMF). [b]Calculated by $^1$H NMR.

**Synthesis of a Complementary Small Supramolecular Chromophore Py-T.** To probe the behavior of the multiple hydrogen bonding base pairs, a T-functionalized pyrene derivative Py-T was synthesized through a click reaction of Py-$N_3$, obtained from commercially available 1-pyrenemethanol according to our previously reported procedure,[24] with PT, forming the complementary supramolecular chromophore as a yellowish powder in 85% yield. The signal for azide stretching at 2100 $cm^{-1}$ in the FTIR spectrum of Py-$N_3$ disappeared completely after triazole ring formation (Figure S4). The signals of the protons of the $CH_2$ unit neighboring the azide group in Py-$N_3$ (at 5.21 ppm) and the $CH_2$ unit neighboring the terminal alkyne group in PT (at 4.56 ppm) both shifted downfield once the triazole had formed. After the click reaction, three characteristic signals appeared in the $^1$H NMR spectrum (Figure S5): for the triazole proton (at 8.04 ppm) and for the two $CH_2$ groups adjacent to the triazole moiety (at 6.35 and 4.84 ppm, respectively). Signals appeared in the $^{13}$C NMR spectrum at 142.7, 122.7, 50.8, and 42.1 ppm for the carbon atoms surrounding of the newly formed triazole ring (Figure S6). The combined NMR and FTIR spectral data confirmed the successful modification of the pyrene derivative.

**Conformations of PPLG and PPLG-DAP Polymers.** Polypeptides are fascinating materials because of their unique secondary structures. It has been reported that polypeptides with different numbers of repeat units can exist in different conformations.[28] To understand this effect more deeply, we designed a series of PPLGs having DPs of 10, 30, and 60, respectively. The signals in the GPC traces of these three polypeptides were clearly separated, with small PDIs resulting from the controlled ROP (Figures 4a–c). MALDI-TOF mass



DOI: 10.1021/acs.macromol.6b01060
Macromolecules 2016, 49, 5374–5385

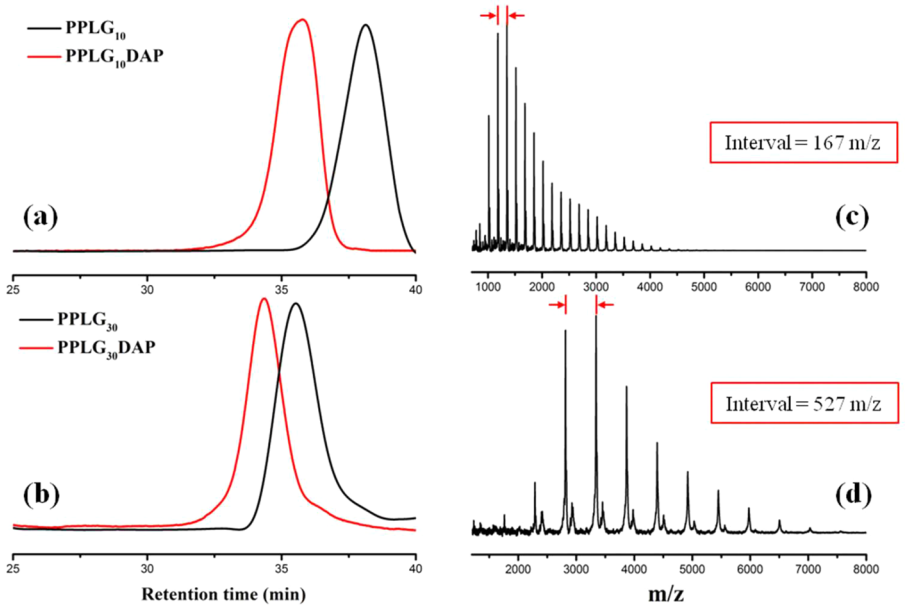


**Figure 3.** GPC traces of (a) $PPLG_{10}$ (red line) and $PPLG_{10}DAP$ (black line) and (b) $PPLG_{30}$ (red line) and $PPLG_{30}DAP$ (black line). MALDI-TOF mass spectra of (c) $PPLG_{10}$ and (d) $PPLG_{10}DAP$.

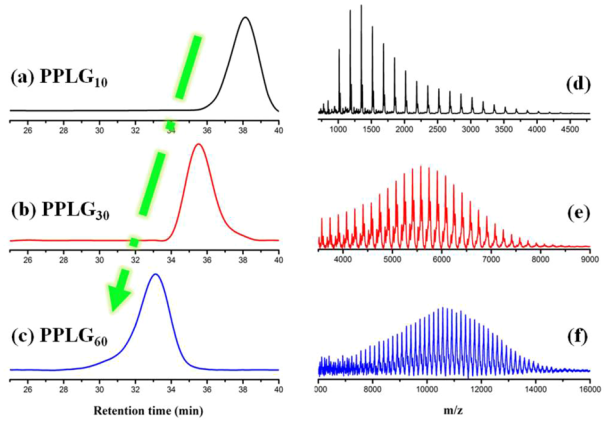


**Figure 4.** (a–c) GPC traces and (d–f) MALDI-TOF mass spectra of (a, d) $PPLG_{10}$, (b, e) $PPLG_{30}$, and (c, f) $PPLG_{60}$.

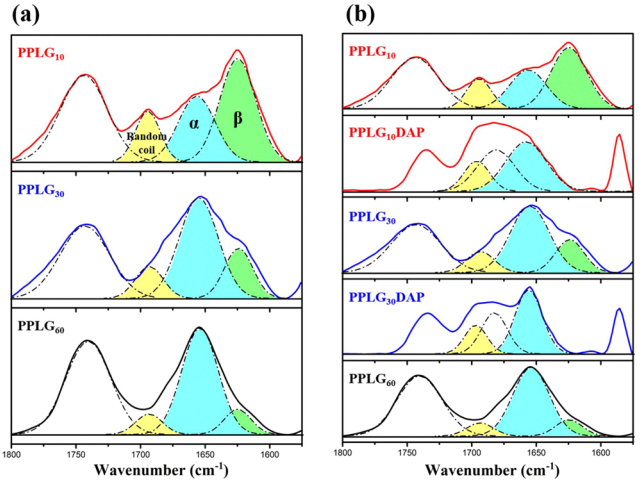


**Figure 5.** FTIR spectra of (a) $PPLG_{10}$, $PPLG_{30}$, and $PPLG_{60}$ and (b) $PPLG_{10}$, $PPLG_{10}DAP$, $PPLG_{30}$, $PPLG_{30}DAP$, and $PPLG_{60}$ (the fitting curve at 1682 $cm^{-1}$ was contributed by the signal of the amide group from the DAP moieties).

spectra of these polypeptides all featured signals with expected statistical distributions and a signal interval of $m/z$ 167, consistent with the structure of each repeat unit (Figures 4d–f). Similar trends were evident in both the GPC traces and MALDI-TOF mass spectra: that is, $PPLG_{10}$, $PPLG_{30}$, and $PPLG_{60}$ all provided similar peak shapes but had different molecular weights. It is practical to ensure that the polymeric samples used for comparison have similar low PDIs to minimize any structural interference from oligomers.

FTIR spectroscopy is a useful technique for probing the structures of materials in the solid state. The FTIR spectra in Figure 5a were first deconvoluted using the second-derivative technique,[29] and the fraction for each secondary structure was calculated and collected in Table 2. For PPLG, strong intramolecular hydrogen bonding in the polymer backbone may lead to an $\alpha$-helical secondary structure, whereas intermolecular hydrogen bonding may lead to a $\beta$-sheet structure. In addition, random coil structures are sometimes observed for various peptide systems.[30] A series of Gaussian distributed curves were fitted to the amide I region (Figure 5a). The amide I region of $PPLG_{10}$ was dominated by the $\beta$-sheet conformation (1627 $cm^{-1}$, lime-colored area); the fraction of $\alpha$-helical structures (1655 $cm^{-1}$, cyan-colored area) increased upon increasing the DP. For $PPLG_{30}$ and $PPLG_{60}$, the amide I region revealed mainly the $\alpha$-helical signal, with only low

**Table 2. Fractions of Each Secondary Structures of Polypeptides Used in This Study**

| sample | $PPLG_{10}$ | $PPLG_{10}DAP$ | $PPLG_{30}$ | $PPLG_{30}DAP$ | $PPLG_{60}$ |
|---|---|---|---|---|---|
| fraction of $\alpha$-helix[a] [%] | 32.0 | 69.0 | 62.9 | 72.6 | 76.8 |
| fraction of $\beta$-sheet[a] [%] | 47.6 | | 22.8 | | 12.8 |
| fraction of random coil[a] [%] | 20.4 | 31.0 | 14.3 | 27.4 | 10.4 |

[a]Calculated from deconvoluted FT-IR data in the region of 1550–1800 $cm^{-1}$.



DOI: 10.1021/acs.macromol.6b01060
Macromolecules 2016, 49, 5374–5385

fractions of the other structures, including the random coil conformation (1694 $cm^{-1}$, yellow-colored area). Preference for an $\alpha$-helical conformation is usually observed in high-DP polypeptides, while both structures can be observed for low-DP polypeptides (DP < 18).[31] Figure 5b presents an overlay of the spectra of these polypeptides before and after the click reactions. An interesting phenomenon is evident for $PPLG_{10}DAP$ in comparison with $PPLG_{10}$: the conformation changed from $\beta$-sheet- to $\alpha$-helical-dominant. The $\alpha$-helical-dominant peak became more obvious for $PPLG_{30}DAP$, with complete disappearance of the $\beta$-sheet conformation in the fitting results. This phenomenon may have been caused by structural interference from the long side chains provided by Az-DAP; that is, the long alkyl spacer and strongly multiple hydrogen-bonding DAP moiety suppressed the interchain hydrogen-bonding interaction (between C═O groups and the amide linkages) in the polypeptide backbone, thereby leading to the preferred intrachain $\alpha$-helical conformation.[32] Thus, we had successfully formed polyglutamates with $\alpha$-helical-dominant structures even when the DP was less than 18.

Because most biomaterials found in nature have poor solubility in organic solvents and low crystallinity, their conformational studies are often performed in the solid state, making it difficult to compare their structures with those of other materials. Nevertheless, $^{13}C$ solid state CP/MAS NMR spectroscopy is a powerful protocol for characterizing these amorphous materials. For PPLGs, the signals of the $C_\alpha$ and amide C═O carbon nuclei are affected by the local conformations of each amino acid residue, reflecting the competition between inter- and intramolecular hydrogen bonding. As displayed in Figure 6, the signal of the terminal

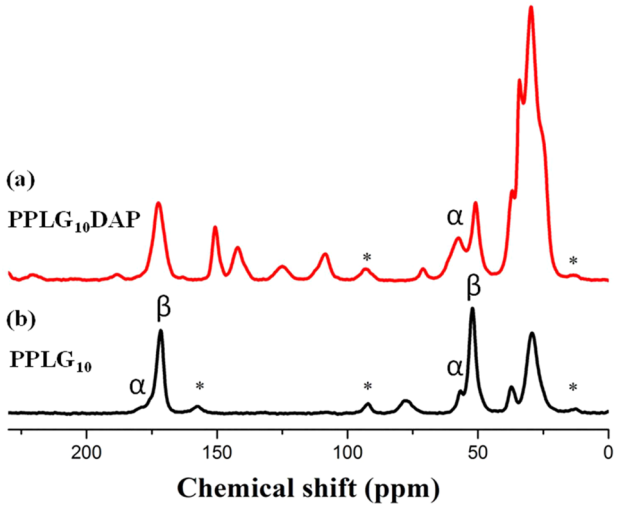


**Figure 6.** $^{13}C$ CP/MAS solid state NMR spectra of (a) $PPLG_{10}DAP$ and (b) $PPLG_{10}$ [asterisk represents spinning sidebands (SSBs)].

alkyne carbon atom at 77 ppm disappeared while a series of new peaks appeared arising from Az-DAP and the newly formed 1,2,3-triazole ring, consistent with the results from the solution state NMR spectra and FT-IR results, confirming the synthesis of PPLG-DAP. It has been reported that the $\alpha$-helical conformation provides signals with chemical shifts of 57.5 ppm ($C_\alpha$) and 176 ppm (C═O), whereas the signals are shifted upfield by approximately 4−5 ppm in the $\beta$-sheet structure.[31] The $^{13}C$ CP/MAS spectrum of $PPLG_{10}$ featured a group of signals at 52 and 171.8 ppm for $\beta$-sheet structures as well as another group of signals for $\alpha$-helical structures at 57.5 and 176 ppm. Higher fractions of the former group of signals were evident for the $\beta$-sheet-dominant conformation of $PPLG_{10}$. In contrast, the fraction of $\alpha$-helical structures increased after postfunctionalization. The signal for the $C_\alpha$ nuclei at 57.5 ppm became more obvious and distinct from the other signals. A partial overlap occurred, however, for the $\beta$-sheet and Az-DAP signals in the C═O region. With an $\alpha$-helical-dominant structure of $PPLG_{10}DAP$ identified from the different positions of the C═O and $C_\alpha$ resonances of its two secondary structures, we used wide-angle X-ray scattering (WAXS) to identify and confirm the different secondary structure of the PPLG and PPLG-DAP polymers.

An extended side chain may affect the secondary structure of a PPLG polymer. In Figure 7, the WAXS spectrum of $PPLG_{10}$

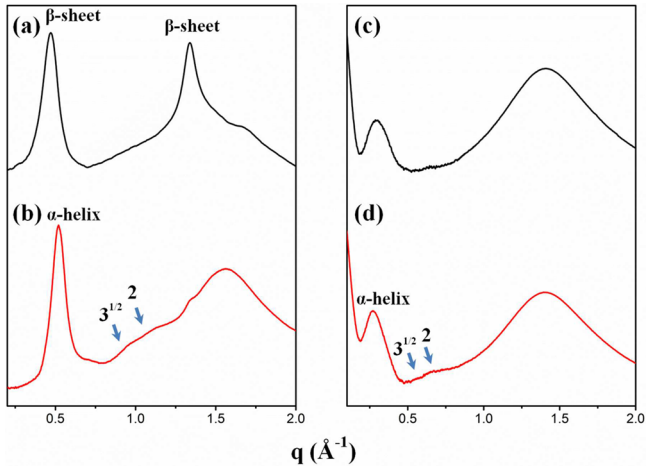


**Figure 7.** WAXS profiles (collected at 373 K) of (a) $PPLG_{10}$, (b) $PPLG_{30}$, (c) $PPLG_{10}DAP$, and (d) $PPLG_{30}DAP$.

displays strong signals for the $\beta$-sheet secondary structure. The first sharp peak appears at a value of $q$ of 0.47, corresponding to the distance ($d$ = 1.33 nm) between the backbones in the antiparallel $\beta$-pleated sheet conformation. Another Bragg peak centered at a value of $q$ of 1.34 ($d$ = 0.470 nm) represented the distance between neighboring peptide chains in one lamella.[33] In the WAXS spectrum of $PPLG_{30}$ (Figure 7b), the primary peak ($q^*$) shifted to higher angle compared with that of $PPLG_{10}$. The $q^*$ signal and the other two signals formed a $1:3^{1/2}:2$ permutation, a typical indication of an $\alpha$-helical structure. Generally, these three peaks represent the (10), (11), and (20) reflections of a two-dimensional (2D) hexagonal cylindrical packing with a cylinder distance of 1.18 nm, due to the formation of nematic-like paracrystals with a periodic packing of 18/5 $\alpha$-helices.[31] Compared with $PPLG_{10}$, the postfunctionalized $PPLG_{10}DAP$ exhibited a totally distinct WAXS profile (Figures 7c and 7d). The sharp peak of the original $\beta$-sheet conformation was replaced by one for a newly formed $\alpha$-helical structure. In addition, a broad amorphous region appeared at a value of $q$ of 1.39 due to the long amorphous side chains introduced into the polypeptide.[34] The signal was more clear in the profile for $PPLG_{30}DAP$, which also displayed the $1:3^{1/2}:2$ permutation of the positions. After the click reactions, the PPLG-DAP polymers featured mainly $\alpha$-helical secondary structures with the primary peaks appearing at a value of $q$ of 0.27, related to 2D hexagonal cylindrical packing with a distance of 2.01 nm.



DOI: 10.1021/acs.macromol.6b01060
Macromolecules 2016, 49, 5374−5385

In brief, from FT-IR spectra and WAXS data, $PPLG_{10}$, $PPLG_{30}$, $PPLG_{60}$ show a trend that with the increase of molecular weight the amount of $\alpha$-helix increased (especially compared between PPLGs with DP < 18 and DP > 18) while the amount of $\beta$-sheet and random coil decreased. In addition, the postfunctionalized supramolecular polypeptides PPLG-DAPs also exhibited higher fraction of $\alpha$-helix compared with PPLGs as a result for $^{13}C$ CP/MAS spectra and WAXS analyses. The combined results from the FTIR spectra, $^{13}C$ CP/MAS spectra, and WAXS experiments suggested that a preference for $\alpha$-helical conformations was induced upon incorporation of DAP moieties on the side chains of the PPLG polymers. According to the analyses mentioned above, we found that the preference of different polypeptide secondary structures can be adjusted by changes in both molecular weight and the strength of inter/intramolecular hydrogen-bonding interactions.

**Thermal Properties of Polypeptides and Recognition of DAP···T Base Pairs.** In our previous publication we reported that the introduction of strong multiple hydrogen-bonding motifs can lead to large improvements in a polymer's thermal properties.[35] To verify this phenomenon, we used DSC to measure the thermal properties of our new PPLG and PPLG-DAP polymers (Figure 8). No obvious melting or crystallization behavior appeared in the DSC thermogram of PPLG, evidence for its low crystallinity. The original glass transition temperatures ($T_g$) of $PPLG_{10}$ and $PPLG_{30}$ were 26.5 and 26.8 °C, as reported previously.[36] After the click reactions, the supramolecular functionalized $PPLG_{10}DAP$ and $PPLG_{30}DAP$ polymers displayed values of $T_g$ of 59.2 and 60.6 °C, respectively. These large increases in the values of $T_g$ arose mainly from the strong hydrogen-bonding interactions of the DAP moieties. These hydrogen bonds are highly self-complementary, leading to the formation of physically cross-linked networks and therefore restricted molecular chain motion.[37] The incorporation of DAP units can also enhance the thermal responsivity of a material. The dynamic interactions of these supramolecular materials can induce properties of responsivity and reversibility that are rarely found in covalently bonded materials. We used variable-temperature $^1H$ NMR spectroscopy to examine these properties (Figure S7). The signal of the NH unit of $PPLG_{10}DAP$ appeared at 10.16 ppm at 25 °C, indicative of strong association through self-complementary DAP···DAP hydrogen bonding. Upon heating, the NH signal gradually shifted upfield and broadened, reaching a final position at 9.53 ppm at 100 °C, suggesting that dissociation had occurred to achieve an equilibrium state at this high temperature.[38] Upon subsequent cooling, the signal of the NH unit shifted back to its original position (10.16 ppm). The reversibility of the position of the NH chemical shift is evidence for dissociation and reassociation processes being available in this current system. The thermal stabilities of our polypeptides were studied using variable-temperature FTIR spectroscopy. Figures 9a and 9b summarize the variable-temperature FTIR spectral data for $PPLG_{30}$ and $PPLG_{30}DAP$ in the amide I and amide II regions. $PPLG_{30}$ exhibited an inherent $\alpha$-helical structure with low fractions of $\beta$-sheet and random coil conformations at room temperature, as mentioned earlier. As the temperature increased, the signal of the $\alpha$-helical conformation (1655 $cm^{-1}$) decreased and broadened, reflecting the dissociation of C═O···NH units in the peptide backbone. In addition, the intensity of the signal for the $\beta$-sheet structures at 1627 $cm^{-1}$ increased, finally reaching equal abundance with that for the $\alpha$-helical conformations at 160 °C. In the amide II region, the signal at 1546 $cm^{-1}$, corresponding to the $\alpha$-helical structures, disappeared gradually, a similar trend to that observed in the amide I region. In contrast, $PPLG_{30}DAP$, which adopted only the $\alpha$-helical conformation at room temperature, was insensitive to the temperature. This unexpected behavior of $PPLG_{30}DAP$ suggests that the strong self-assembled network induced by the multiple hydrogen-bonding DAP motifs could stabilize the secondary structure of the polypeptide significantly, even at a low DP. Thus, the attachment of functionalities capable of multiple hydrogen-bonding interactions improved the thermal properties of the polypeptides and provided additional stability against variations in temperature.

The strong multiple hydrogen bonding of DAP···T base pairs can lead to properties that are rarely found in covalently bonded materials. Supramolecular complexes were produced from this molecular recognition behavior, as evidenced in the variable-temperature $^1H$ NMR spectra in Figure 9c. The signal for the amide proton of Py-T appeared at 8.15 ppm in TCE, a nonpolar medium; it shifted to 9.05 ppm upon molecular recognition of the T moiety of Py-T with the DAP moieties of $PPLG_{30}DAP$, revealing that this heterocomplementary base pair could efficiently lead to the formation of a supramolecular complex. In addition, the thermoresponsivity of the supramolecular complex was evident in variable-temperature spectra. As the temperature increased, the hydrogen bonds in the complex dissociated, with a gradual shifting trend observed in the overlaid spectra.[23] The supramolecular complex revealed reversibility in its hydrogen-bonding behavior upon cooling to

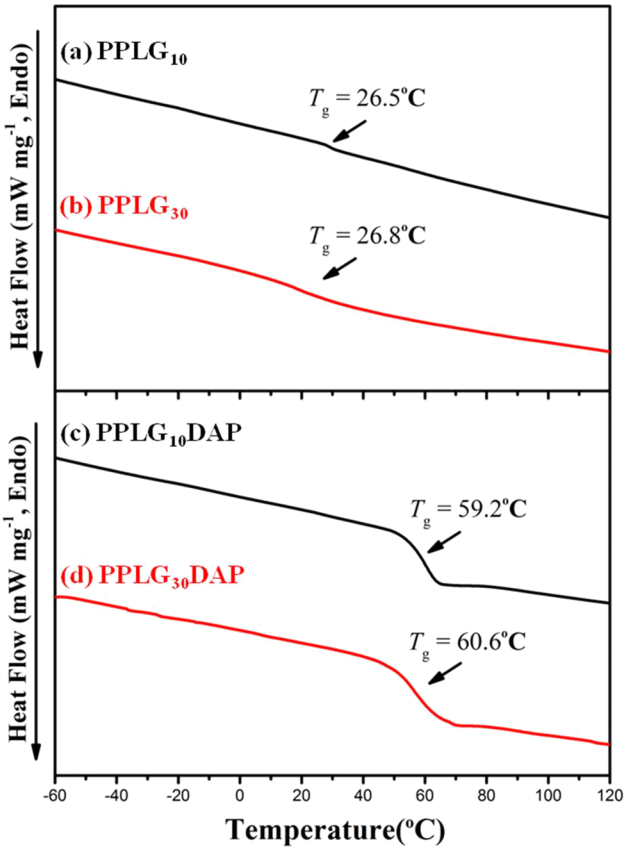


**Figure 8.** DSC thermograms of (a) $PPLG_{10}$, (b) $PPLG_{30}$, (c) $PPLG_{10}DAP$, and (d) $PPLG_{30}DAP$.


DOI: 10.1021/acs.macromol.6b01060
Macromolecules 2016, 49, 5374−5385

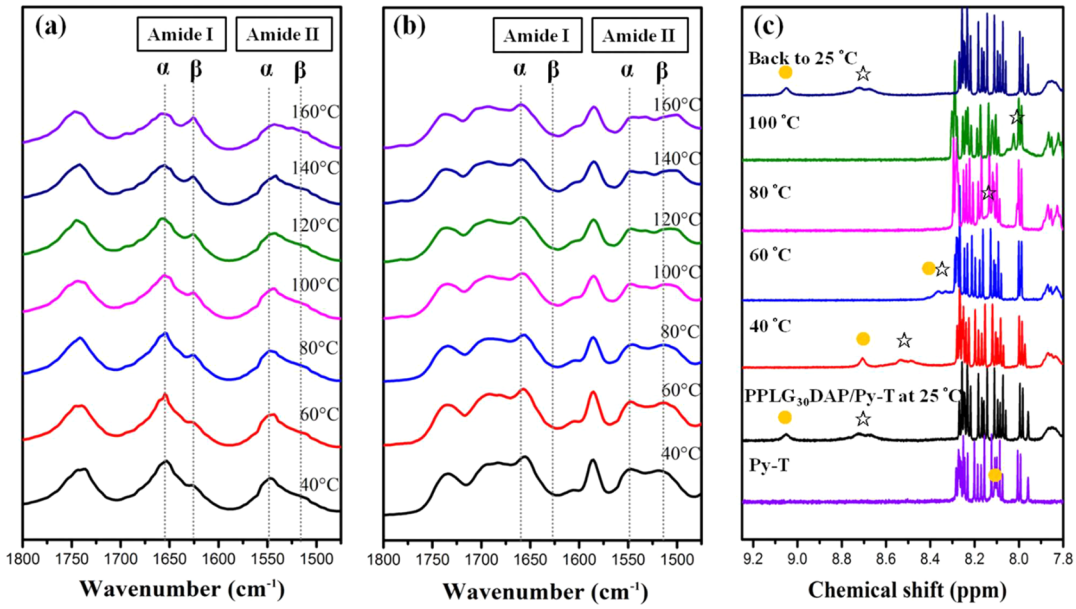


**Figure 9.** (a, b) Variable-temperature FTIR spectra of (a) $PPLG_{30}$ and (b) $PPLG_{30}DAP$. (c) Partial variable-temperature $^1H$ NMR spectra of Py-T and $PPLG_{30}DAP$/Py-T (molar ratio, 1:1) at different temperatures in 1,1,2,2-tetrachloroethane-$d_2$ (● represents amide proton signal from T unit; ☆ represents amide proton signal from DAP moieties).

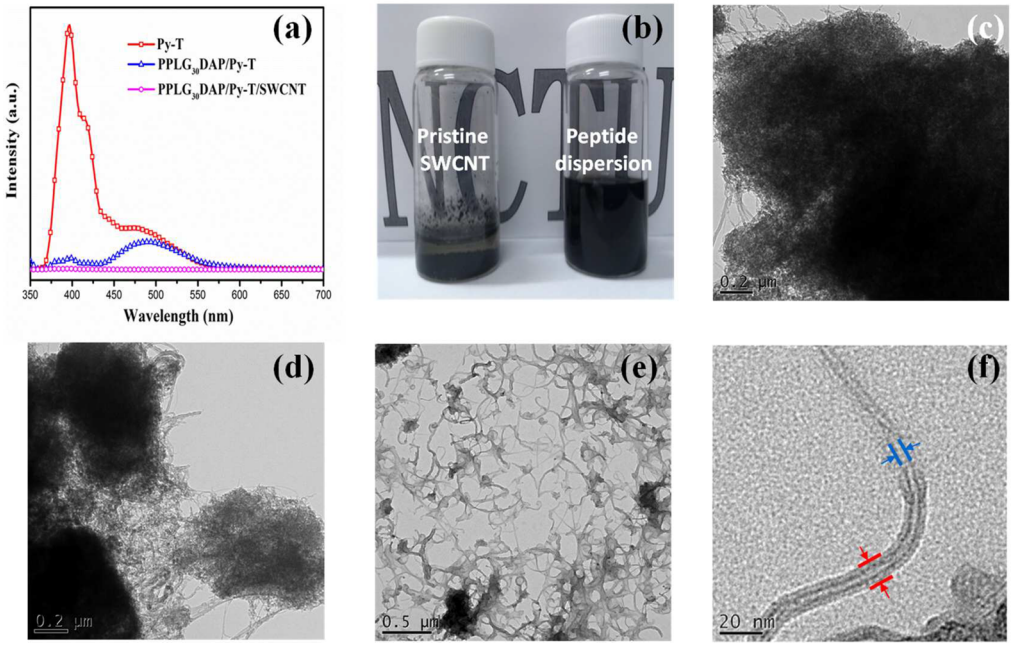


**Figure 10.** (a) Overlay of PL emission spectra for different pyrene-containing species in DMF ($10^{-3}$ M). (b) Photographs of pristine SWCNT and $PPLG_{30}DAP$/Py-T/SWCNT dispersions in DMF. (c–g) TEM images of (c, d) pure SWCNTs after sonication in DMF and (e, f) $PPLG_{30}DAP$/Py-T/SWCNT dispersions on (e) large and (f) small scales.

room temperature. The signals of the DAP and T protons appeared in same position as they had originally, evidence for the reversibility of the molecular recognition process through heat treatment, thereby ensuring the stability of the $PPLG_{30}DAP$/Py-T supramolecular complex.

**Using Supramolecular Complexes for CNT Dispersion and CNT Composite Fabrication.** CNTs are among the most difficult materials to disperse because the strong $\pi$-stacking between the tubes can readily form aggregates that precipitate. Supramolecular complexes can be effective dispersing agents for CNTs because of the specificity of their noncovalent interactions.[35,39] Use simple methodology, we can provide extra possibility for more applications on polypeptide matrix. Since polypeptide itself have no (or weak) interaction with CNT, the introduction of molecules with $\pi-\pi$ stacking ability (e.g., pyrene unit) may be a strategy to increase the dispersity. In addition, to increase the miscibility between PPLG and pyrene molecule (which were two immiscible components under normal condition), we choose strong recognized base pair DAP-T to perform the blending material. Here, we examined the applicability of our PPLG-DAP/Py-T supramolecular complex for CNT dispersion. Figure 10 displays


DOI: 10.1021/acs.macromol.6b01060
Macromolecules 2016, 49, 5374–5385

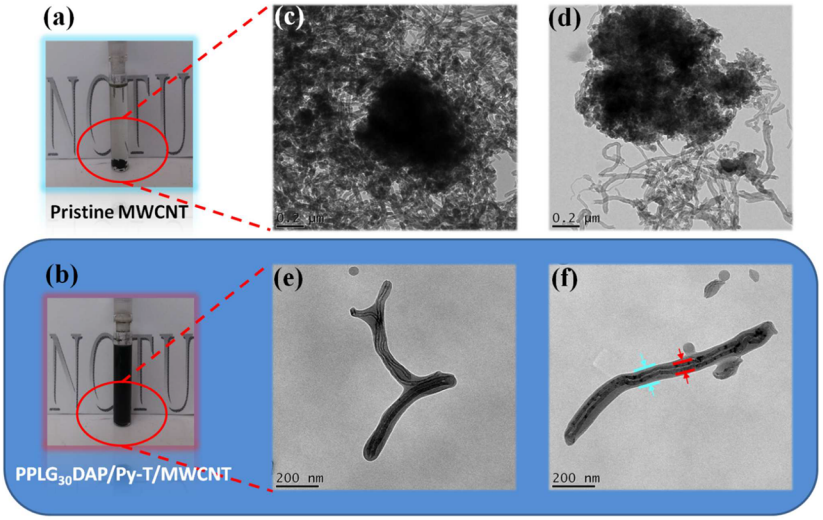


**Figure 11.** Photographs of (a) pristine MWCNT and (b) $PPLG_{30}DAP/Py\text{-}T/MWCNT$ dispersions in TCE. TEM images of (c, d) pure MWCNT after sonication in TCE and (e, f) the $PPLG_{30}DAP/Py\text{-}T/MWCNT$ dispersion.

the results for SWCNT dispersion. First, PL emission spectra were recorded to determine whether Py-T played an important role in the ternary blending system or not. Under excitation at 343 nm, Py-T exhibited both strong monomeric fluorescence (374 nm) and eximeric fluorescence (493 nm), while $PPLG_{30}DAP/Py\text{-}T$ exhibited mainly eximeric emission (Figure 10a) because of the presence of the side chain pyrene unit. In contrast, the $PPLG_{30}DAP/Py\text{-}T/SWCNT$ dispersion displayed nearly no emission in the visible light region, suggesting that energy transfer occurred effectively between the light-emitted pyrene unit and the SWCNTs.[24,40] The quenching effect presumably occurred because most of the pyrene units were interacting with the CNTs through $\pi$-stacking. Further evidence for this behavior is evident in Figure 10b, which displays photographs of the pristine SWCNT dispersion and $PPLG_{30}DAP/Py\text{-}T/SWCNT$ supramolecular dispersion in DMF after sonication and standing at room temperature for 24 h. It has been reported that only solvents that are Lewis bases or amides [e.g., DMF, *N*-methylpyrrolidone (NMP)] have the ability to readily disperse pure SWCNTs.[41] Nevertheless, because of the strong interactions between the SWCNTs, these dispersions still form aggregates on the time scale of several days.[42] Similar behavior was evident in our control experiment, with the pristine SWCNTs precipitating 24 h after dispersion in DMF (Figure 10b). In contrast, the supramolecular dispersion of SWCNTs did not form any obvious precipitate. The stability of this dispersion arose mainly from the hydrogen bonding of the DAP···T base pairs and the $\pi-\pi$ interactions between the pyrene units and the walls of the CNTs. A clear picture of these stabilizing interactions is revealed in the TEM images of these samples. As displayed in Figures 10c–f, the pristine SWCNTs in DMF underwent serious aggregation on the scale of several micrometers, while the supramolecular dispersion led to effective separation of the aggregated SWCNTs through the combination of noncovalent interactions. More importantly, the dispersion was stable for several months, potentially providing additional convenience to further manufacturing processes.

The main feature of the $PPLG_{30}DAP/Py\text{-}T$ supramolecular complex is its ability to interact with $\pi$-conjugated units. Thus, we tested the use of this complex to also fabricate MWCNT-based nanocomposites. The dispersion method used was similar to that for the dispersion of the SWCNTs, but to examine whether the supramolecular complex could increase the solubility in organic solvents, we changed the dispersing medium to TCE. In TCE, hydrogen-bonding species can interact with complementary units without interference from the solvent molecules. In contrast to the situation for the SWCNTs in DMF, the pristine MWCNTs in TCE formed a serious precipitate within 1 h because of the lack of polarity and amine electron donation (Figure 11a); again, the supramolecular dispersion remained stable after 6 months (Figure 11b). TEM images revealed the structures formed within the dispersions. As observed for the SWCNT/DMF system, the MWCNTs without functionalization or surfactant molecules present readily formed large-scale aggregates and precipitates with new equilibrium state of low energy (Figures 11c and 11d).[42] In contrast, the supramolecular complex present in the system played the role of a surfactant, using steric hindrance or static charge repulsion to effectively stabilize the CNTs,[42] forming shell-like structures around the walls of the MWCNTs and preventing their reaggregation driven by van der Waals attraction (Figures 11e and 11f). The resulting dispersion was dried under vacuum to remove all of the solvent and isolate the supramolecular/CNT composite; TGA was then used to examine the composite's properties (Figure S8). Assuming that the weight loss behavior was similar to that of the individual supramolecular complex and MWCNT, the content of MWCNT, calculated from the char yields measured through TGA, was 54.87%. Figure 12 presents DSC thermograms of the polypeptides, the supramolecular complex, and the MWCNT composite; Table 3 lists the related properties. After functionalizing with the DAP moieties, the value of $T_g$ increased from 26.8 to 60.8 °C because of the dominant behavior of the self-complementary physical cross-linked network, as discussed earlier. Once the supramolecular complex had formed between $PPLG_{30}DAP$ and Py-T, the value of $T_g$ again increased, to 77.2 °C, presumably because the heterocomplementary hydrogen bonding of the DAP···T base pair and the $\pi$-stacking of the pyrene units limited the molecular motion of the polymer backbone. These shifts in the values of $T_g$ suggested that strong molecular recognition was


DOI: 10.1021/acs.macromol.6b01060
*Macromolecules* 2016, 49, 5374–5385

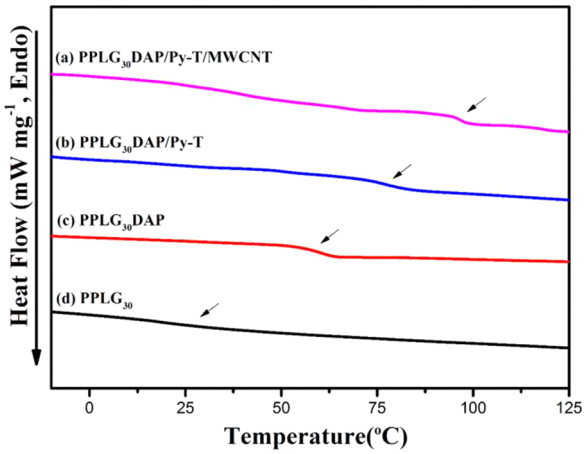


**Figure 12.** DSC thermograms of (a) $PPLG_{30}DAP$/Py-T/MWCNT, (b) $PPLG_{30}DAP$/Py-T, (c) $PPLG_{30}DAP$, and (d) $PPLG_{30}$.

**Table 3. Thermal Properties of the Materials Used in This Study**

| samples | MWCNT | $PPLG_{30}DAP$/Py-T/MWCNT | $PPLG_{30}DAP$/Py-T | $PPLG_{30}DAP$ |
|---|---|---|---|---|
| char yield at 600 °C[a] (wt %) | 97.28 | 67.38 | 31.02 | 14.24 |
| MWCNT content[a] (wt %) | 100 | 54.87 | 0 | 0 |
| $T_g$[b] (°C) | | 96.5 | 77.2 | 60.6 |

[a]Measured by TGA. [b]Calculated by DSC.

occurring. The shift in the value of $T_g$ became even more significant for the $PPLG_{30}DAP$/Py-T/MWCNT composite because of enhanced steric hindrance resulting from the rigid and bulky CNT structure and the surface adsorption of the pyrene units restricting the segmental motion of the polymer backbone. Thus, the thermal properties of these composites may have an additional level of fine-tuning, either through varying the amount of the supramolecular complex or through simple adjustment of the CNT loading content. A variety of polymeric materials could be applied using this strategy, potentially greatly improving the processability of nonfunctionalized CNTs.

## CONCLUSION

A new series of polypeptides presenting multiple hydrogen-bonding moieties have been synthesized using a simple sequence of reactions. The progress of the postfunctionalization step was examined using NMR, FTIR, and MALDI-TOF mass spectra. A conformational study was performed to determine the effect of the side-chain functionality on the polypeptide's secondary structure. FTIR spectral deconvolution and solid state $^{13}C$ NMR and WAXS spectra revealed that after Az-DAP had been grafted onto either the $\beta$-sheet or $\alpha$-helical polypeptides, the $\alpha$-helical secondary structure became dominant due to the long alkyl spacers and the strong interactions between DAP base pairs. The presence of the DAP units also affected the thermal properties of the polymers, with the resulting physical cross-linked network enhancing the value of $T_g$ by approximately 34 °C relative to that of the pristine PPLG. The thermal stability of the PPLG-DAP polymers was also greater than that of the PPLGs, allowing them to sustain their unique architectures. In addition, supramolecular complexes were prepared through molecular recognition to exploit secondary noncovalent bonding interactions. Thus, pyrene units were presented peripherally to facilitate the dispersion of CNTs through $\pi-\pi$ interactions. The combination of hydrogen bonding and $\pi$-stacking generated stable dispersions of CNTs in both polar and nonpolar media, expanding the possibilities of dispersing strategies. Alternatively, polypeptide/CNT composites with high glass transition temperatures may find wider practicality, exploiting their useful optoelectronic properties, in biomedical applications.

## ASSOCIATED CONTENT

### Supporting Information

The Supporting Information is available free of charge on the ACS Publications website at DOI: 10.1021/acs.macromol.6b01060.

The detail synthesis part such as Scheme S1, PPLG, PPLG-DAP, Py-T, and the additional characterization data (Figures S1–S8) (PDF)

## AUTHOR INFORMATION

### Corresponding Author

*E-mail: kuosw@faculty.nsysu.edu.tw (S.-W.K.).

### Notes

The authors declare no competing financial interest.

## ACKNOWLEDGMENTS

This study was supported financially by the Ministry of Science and Technology, Taiwan, under Contracts MOST103-2221-E-110-079-MY3 and MOST102-2221-E-110-008-MY3. Special thanks to Mr. Hsien-Tsan Lin of the Regional Instruments Center at National Sun Yat-Sen University for help with the TEM measurement. The authors also want to thank Dr. Yung-Chih Lin at National Sun Yat-Sen University for valuable discussions.

## REFERENCES

(1) (a) Philp, D.; Stoddart, J. F. Self-Assembly in Natural and Unnatural Systems. *Angew. Chem., Int. Ed. Engl.* **1996**, *35*, 1154. (b) Mai, Y. Y.; Eisenberg, A. Self-Assembly of Block Copolymers. *Chem. Soc. Rev.* **2012**, *41*, 5969. (c) Huang, F. H.; Anslyn, E. V. Introduction: Supramolecular Chemistry. *Chem. Rev.* **2015**, *115*, 6999.

(2) (a) Whitesides, G. M.; Boncheva, M. Beyond molecules: Self-Assembly of Mesoscopic and Macroscopic Components. *Proc. Natl. Acad. Sci. U. S. A.* **2002**, *99*, 4769. (b) Sary, N.; Richard, F.; Brochon, C.; Leclerc, N.; Lévêque, P.; Audinot, J.-N.; Berson, S.; Heiser, T.; Hadziioannou, G.; Mezzenga, R. A New Supramolecular Route for Using Rod-Coil Block Copolymers in Photovoltaic Applications. *Adv. Mater.* **2010**, *22*, 763. (c) Du, P.; Liu, J. H.; Chen, G. S.; Jiang, M. Dual Responsive Supramolecular Hydrogel with Electrochemical Activity. *Langmuir* **2011**, *27*, 9602. (d) Yan, X. Z.; Xu, D. H.; Chi, X. D.; Chen, J. Z.; Dong, S. Y.; Ding, X.; Yu, Y. H.; Huang, F. H. A Multiresponsive, Shape-Persistent, and Elastic Supramolecular Polymer Network Gel Constructed by Orthogonal Self-Assembly. *Adv. Mater.* **2012**, *24*, 362. (e) Wang, G. T.; Tang, B. H.; Liu, Y.; Gao, Q. Y.; Wang, Z. Q.; Zhang, X. The Fabrication of a Supra-Amphiphile for Dissipative Self-Assembly. *Chem. Sci.* **2016**, *7*, 1151.

(3) (a) Shandryuk, G. A.; Kuptsov, S. A.; Shatalova, A. M.; Plate, N. A.; Talroze, R. V. Liquid Crystal H-Bonded Polymer Networks under Mechanical Stress. *Macromolecules* **2003**, *36*, 3417. (b) Pollino, J. M.; Weck, M. Non-Covalent Side-Chain Polymers: Design Principles, Functionalization Strategies, and Perspectives. *Chem. Soc. Rev.* **2005**,



DOI: 10.1021/acs.macromol.6b01060
*Macromolecules* 2016, 49, 5374–5385

34, 193. (c) Burd, C.; Weck, M. Self-Sorting in Polymers. *Macromolecules* **2005**, *38*, 7225. (d) Nykänen, A.; Nuopponen, M.; Laukkanen, A.; Hirvonen, S.-P.; Rytelä, M.; Turunen, O.; Tenhu, H.; Mezzenga, R.; Ikkala, O.; Ruokolainen, J. Phase Behavior and Temperature-Responsive Molecular Filters Based on Self-Assembly of Polystyrene-*block*-poly(N-isopropylacrylamide)-*block*-polystyrene. *Macromolecules* **2007**, *40*, 5827. (e) Hammond, M. R.; Mezzenga, R. Supramolecular Routes Towards Liquid Crystalline Side-Chain Polymers. *Soft Matter* **2008**, *4*, 952. (f) Liu, J. H.; Chen, G. S.; Jiang, M. Supramolecular Hybrid Hydrogels from Noncovalently Functionalized Graphene with Block Copolymers. *Macromolecules* **2011**, *44*, 7682.

(4) (a) Morris, M. C. Fluorescent Biosensors of Intracellular Targets from Genetically Encoded Reporters to Modular Polypeptide Probes. *Cell Biochem. Biophys.* **2010**, *56*, 19. (b) Myung, S.; Yin, P. T.; Kim, C. L.; Park, J. S.; Solanki, A.; Reyes, P. I.; Lu, Y. C.; Kim, K. S.; Lee, K.-B. Label-Free Polypeptide-Based Enzyme Detection Using a Graphene-Nanoparticle Hybrid Sensor. *Adv. Mater.* **2012**, *24*, 6081.

(5) Tian, B.; Tao, X. G.; Ren, T. Y.; Weng, Y.; Lin, X.; Zhang, Y.; Tang, X. Polypeptide-Based Vesicles: Formation, Properties and Application for Drug Delivery. *J. Mater. Chem.* **2012**, *22*, 17404.

(6) (a) Hirano, Y.; Mooney, D. J. Peptide and Protein Presenting Materials for Tissue Engineering. *Adv. Mater.* **2004**, *16*, 17. (b) Jeevithan, E.; Jingyi, Z.; Bao, B.; Shujun, W.; JeyaShakila, R.; Wu, W. H. Biocompatibility Assessment of Type-II Collagen and Its Polypeptide for Tissue Engineering: Effect of Collagen's Molecular Weight and Glycoprotein Content on Tumor Necrosis Factor (Fas/Apo-1) Receptor Activation in Human Acute T-Lymphocyte Leukemia Cell Line. *RSC Adv.* **2016**, *6*, 14236.

(7) (a) Kuo, S. W.; Lee, H. F.; Huang, C. F.; Huang, C. J.; Change, F. C. Self-Assembly and Secondary Structures of Linear Polypeptides Tethered to Polyhedral Oligomeric Silsesquioxane Nanoparticles Through Click Chemistry. *J. Polym. Sci., Part A: Polym. Chem.* **2011**, *49*, 2127. (b) Fu, X. H.; Shen, Y.; Fu, W. X.; Li, Z. B. Thermoresponsive Oligo(ethylene glycol) Functionalized Poly-L-cysteine. *Macromolecules* **2013**, *46*, 3753. (c) Ma, Y. N.; Fu, X. H.; Shen, Y.; Fu, W. X.; Li, Z. B. Irreversible Low Critical Solution Temperature Behaviors of Thermal-responsive OEGylated Poly(L-cysteine) Containing Disulfide Bonds. *Macromolecules* **2014**, *47*, 4684. (d) Sun, L. M.; Fan, Z.; Wang, Y. Z.; Huang, Y. J.; Schmidt, M.; Zhang, M. J. Tunable Synthesis of Self-Assembled Cyclic Peptide Nanotubes and Nanoparticles. *Soft Matter* **2015**, *11*, 3822.

(8) (a) Chen, P.; Li, C.; Liu, D. S.; Li, Z. B. DNA-Grafted Polypeptide Molecular Bottlebrush Prepared via Ring-Opening Polymerization and Click Chemistry. *Macromolecules* **2012**, *45*, 9579. (b) Hu, Q.; Deng, Y.; Yuan, Q. L.; Ling, Y.; Tang, H. Y. Polypeptide Ionic Liquid: Synthesis, Characterization, and Application in Single-Walled Carbon Nanotube Dispersion. *J. Polym. Sci., Part A: Polym. Chem.* **2014**, *52*, 149.

(9) (a) Ajayan, P. M. Nanotubes from Carbon. *Chem. Rev.* **1999**, *99*, 1787. (b) De Volder, M. F. L.; Tawfick, S. H.; Baughman, R. H.; Hart, J. Carbon Nanotubes: Present and Future Commercial Applications. *Science* **2013**, *339*, 535. (c) Li, C. X.; Mezzenga, R. The Interplay Between Carbon Nanomaterials and Amyloid Fibrils in Bio-Nanotechnology. *Nanoscale* **2013**, *5*, 6207.

(10) (a) Barone, P. W.; Baik, S.; Heller, D. A.; Strano, M. S. Near-Infrared Optical Sensors Based on Single-Walled Carbon Nanotubes. *Nat. Mater.* **2005**, *4*, 86. (b) Kim, J. H.; Heller, D. A.; Jin, H.; Barone, P. W.; Song, C.; Zhang, J.; Trudel, L. J.; Wogan, G. N.; Tannenbaum, S. R.; Strano, M. S. The Rational Design of Nitric Oxide Selectivity in Single-Walled Carbon Nanotube Near-Infrared Fluorescence Sensors for Biological Detection. *Nat. Chem.* **2009**, *1*, 473.

(11) (a) Cognet, L.; Tsyboulski, D. A.; Rocha, J.-D. R.; Doyle, C. D.; Tour, J. M.; Weisman, R. B. Stepwise Quenching of Exciton Fluorescence in Carbon Nanotubes by Single-Molecule Reactions. *Science* **2007**, *316*, 1465. (b) Heller, D. A.; Pratt, G. W.; Zhang, J.; Nair, N.; Hansborough, A. J.; Boghossian, A. A.; Reuel, N. F.; Barone, P. W.; Strano, M. S. Peptide Secondary Structure Modulates Single-Walled Carbon Nanotube Fluorescence as a Chaperone Sensor for Nitroaromatics. *Proc. Natl. Acad. Sci. U. S. A.* **2011**, *108*, 8544.

(12) (a) Henrard, L.; Hernández, E.; Bernier, P.; Rubio, A. van der Waals Interaction in Nanotube Bundles: Consequences on Vibrational Modes. *Phys. Rev. B: Condens. Matter Mater. Phys.* **1999**, *60*, 8521. (b) Dieckmann, G. R.; Dalton, A. B.; Johnson, P. A.; Razal, J.; Chen, J.; Giordano, G. M.; Munõz, E.; Musselman, I. H.; Baughman, R. H.; Draper, R. K. Controlled Assembly of Carbon Nanotubes by Designed Amphiphilic Peptide Helices. *J. Am. Chem. Soc.* **2003**, *125*, 1770.

(13) Wang, S.; Humphreys, E. S.; Chung, S. Y.; Delduco, D. F.; Lustig, S. R.; Wang, H.; Parker, K. N.; Rizzo, N. W.; Subramoney, S.; Chiang, Y. M.; Jagota, A. Peptides with Selective Affinity for Carbon Nanotubes. *Nat. Mater.* **2003**, *2*, 196.

(14) Yao, Y.; Li, W.; Wang, S.; Yan, D.; Chen, X. Polypeptide Modification of Multiwalled Carbon Nanotubes by a Graft-From Approach. *Macromol. Rapid Commun.* **2006**, *27*, 2019.

(15) (a) Chen, J.; Hamon, M. A.; Hu, H.; Chen, Y. S.; Rao, A. M.; Eklund, P. C.; Haddon, R. C. Solution Properties of Single-Walled Carbon Nanotubes. *Science* **1998**, *282*, 95. (b) Bahr, J. L.; Yang, J. P.; Kosynkin, D. V.; Bronikowski, M. J.; Smalley, R. E.; Tour, J. M. Functionalization of Carbon Nanotubes by Electrochemical Reduction of Aryl Diazonium Salts: A Bucky Paper Electrode. *J. Am. Chem. Soc.* **2001**, *123*, 6536.

(16) (a) Strano, M. S.; Moore, V. C.; Miller, M. K.; Allen, M. J.; Haroz, E. H.; Kittrell, C.; Hauge, R. H.; Smalley, R. E. The Role of Surfactant Adsorption During Ultrasonication in the Dispersion of Single-Walled Carbon Nanotubes. *J. Nanosci. Nanotechnol.* **2003**, *3*, 81. (b) Islam, M. F.; Rojas, E.; Bergey, D. M.; Johnson, A. T.; Yodh, A. G. High Weight Fraction Surfactant Solubilization of Single-Wall Carbon Nanotubes in Water. *Nano Lett.* **2003**, *3*, 269. (c) Zou, J. H.; Liu, L. W.; Chen, H.; Khondaker, S. I.; McCullough, R. D.; Huo, Q.; Zhai, L. Dispersion of Pristine Carbon Nanotubes Using Conjugated Block Copolymers. *Adv. Mater.* **2008**, *20*, 2055. (d) Sun, Y.; Fu, W. X.; Li, Z. B.; Wang, Z. H. Tailorable Aqueous Dispersion of Single-Walled Carbon Nanotubes Using Tetrachloroperylene-Based Bolaamphiphiles via Noncovalent Modification. *Langmuir* **2014**, *30*, 8615.

(17) Zorbas, V.; Ortiz-Acevedo, A.; Dalton, A. B.; Yoshida, M. M.; Dieckmann, G. R.; Draper, R. K.; Baughman, R. H.; Jose-Yacaman, M.; Musselman, I. H. Preparation and Characterization of Individual Peptide-Wrapped Single-Walled Carbon Nanotubes. *J. Am. Chem. Soc.* **2004**, *126*, 7222.

(18) Whaley, S. R.; English, D. S.; Hu, E. L.; Barbara, P. F.; Belcher, A. M. Selection of Peptides with Semiconductor Binding Specificity for Directed Nanocrystal Assembly. *Nature* **2000**, *405*, 665.

(19) (a) Stupp, S. I.; LeBonheur, V.; Walker, K.; Li, L. S.; Huggins, K. E.; Keser, M.; Amstutz, A. Supramolecular Materials: Self-Organized Nanostructures. *Science* **1997**, *276*, 384. (b) Huang, F. H.; Nagvekar, D. S.; Zhou, X. C.; Gibson, H. W. Formation of a Linear Supramolecular Polymer by Self-Assembly of Two Homoditopic Monomers Based on the Bis(*m*-phenylene)-32-crown-10/Paraquat Recognition Motif. *Macromolecules* **2007**, *40*, 3561. (c) de Greef, T. F. A.; Meijer, E. W. Materials Science: Supramolecular Polymers. *Nature* **2008**, *453*, 171. (d) Merlet-Lacroix, N.; Rao, J. Y.; Zhang, A. F.; Schlüter, A. D.; Bolisetty, S.; Ruokolainen, J.; Mezzenga, R. Controlling Hierarchical Self-Assembly in Supramolecular Tailed-Dendron Systems. *Macromolecules* **2010**, *43*, 4752. (e) Wojtecki, R. J.; Meador, M. A.; Rowan, S. J. Using the Dynamic Bond to Access Macroscopically Responsive Structurally Dynamic Polymers. *Nat. Mater.* **2011**, *10*, 14. (f) Chen, G. S.; Jiang, M. Cyclodextrin-Based Inclusion Complexation Bridging Supramolecular Chemistry and Macromolecular Self-Assembly. *Chem. Soc. Rev.* **2011**, *40*, 2254. (g) Yan, X. Z.; Wang, F.; Zheng, B.; Huang, F. H. Stimuli-Responsive Supramolecular Polymeric Materials. *Chem. Soc. Rev.* **2012**, *41*, 6042.

(20) (a) Aida, T.; Meijer, E. W.; Stupp, S. I. Functional Supramolecular Polymers. *Science* **2012**, *335*, 813. (b) Jie, K. C.; Zhou, Y. J.; Yao, Y.; Shi, B. B.; Huang, F. H. $CO_2$-Responsive Pillar[5]arene-Based Molecular Recognition in Water: Establishment and Application in Gas-Controlled Self-Assembly and Release. *J. Am. Chem. Soc.* **2015**, *137*, 10472−10475.



DOI: 10.1021/acs.macromol.6b01060
*Macromolecules* 2016, 49, 5374−5385

(21) Llanes-Pallas, A.; Palma, C.-A.; Piot, L.; Belbakra, A.; Listorti, A.; Prato, M.; Samorı, P.; Armaroli, N.; Bonifazi, D. Engineering of Supramolecular H-Bonded Nanopolygons via Self-Assembly of Programmed Molecular Modules. *J. Am. Chem. Soc.* **2009**, *131*, 509.
(22) (a) Liu, L.; Jiang, M. Synthesis of Novel Triblock Copolymers Containing Hydrogen-Bond Interaction Groups via Chemical Modification of Hydrogenated Poly (styrene-*block*-butadiene-*block*-styrene). *Macromolecules* **1995**, *28*, 8702. (b) Barth, J. V.; Weckesser, J.; Cai, C. Z.; Gunter, P.; Burgi, L.; Jeandupeux, O.; Kern, K. Building Supramolecular Nanostructures at Surfaces by Hydrogen Bonding. *Angew. Chem., Int. Ed.* **2000**, *39*, 1230. (c) Yoshimoto, S.; Yokoo, N.; Fukuda, T.; Kobayashi, N.; Itaya, K. Formation of Highly Ordered Porphyrin Adlayers Induced by Electrochemical Potential Modulation. *Chem. Commun.* **2006**, *5*, 500.
(23) Huang, C. W.; Wu, P. W.; Su, W. H.; Zhu, C. Y.; Kuo, S. W. Stimuli-Responsive Supramolecular Materials: Photo-Tunable Properties and Molecular Recognition Behavior. *Polym. Chem.* **2016**, *7*, 795.
(24) (a) Lin, Y. C.; Kuo, S. W. Self-Assembly and Secondary Structures of Linear Polypeptides Tethered to Polyhedral Oligomeric Silsesquioxane Nanoparticles Through Click Chemistry. *J. Polym. Sci., Part A: Polym. Chem.* **2011**, *49*, 2127. (b) Huang, K. W.; Wu, Y. R.; Jeong, K.-U.; Kuo, S. W. From Random Coil Polymers to Helical Structures Induced by Carbon Nanotubes and Supramolecular Interactions. *Macromol. Rapid Commun.* **2013**, *34*, 1530.
(25) (a) Daly, W. H.; Poche, D. The Preparation of N-Carboxyanhydrides of α-Amino Acids Using Bis(Trichloromethyl)-Carbonate. *Tetrahedron Lett.* **1988**, *29*, 5859. (b) Lin, Y. C.; Kuo, S. W. Hierarchical Self-Assembly and Secondary Structures of Linear Polypeptides Graft onto POSS in the Side Chain Through Click Chemistry. *Polym. Chem.* **2012**, *3*, 162.
(26) (a) Marie, A.; Fournier, F.; Tabet, J. C. Characterization of Synthetic Polymers by MALDI-TOF/MS: Investigation into New Methods of Sample Target Preparation and Consequence on Mass Spectrum Finger Print. *Anal. Chem.* **2000**, *72*, 5106. (b) Montaudo, G.; Samperi, F.; Montaudo, M. S. Characterization of Synthetic Polymers by MALDI-MS. *Prog. Polym. Sci.* **2006**, *31*, 277.
(27) (a) Robinson, K. L.; Khan, M. A.; de Paz Báñez, M. V.; Wang, X. S.; Armes, S. P. Controlled Polymerization of 2-Hydroxyethyl Methacrylate by ATRP at Ambient Temperature. *Macromolecules* **2001**, *34*, 3155. (b) Aamer, K. A.; Tew, G. N. RAFT Polymerization of a Novel Activated Ester Monomer and Conversion to a Terpyridine-Containing Homopolymer. *J. Polym. Sci., Part A: Polym. Chem.* **2007**, *45*, 5618. (c) Yang, P. C.; Armes, S. P. Preparation of Well-Defined Poly(2-hydroxyethyl methacrylate) Macromonomers via Atom Transfer Radical Polymerization. *Macromol. Rapid Commun.* **2014**, *35*, 242.
(28) (a) Xiao, C. S.; Zhao, C. W.; He, P.; Tang, Z. H.; Chen, X. S.; Jing, X. B. Facile Synthesis of Glycopolypeptides by Combination of Ring-Opening Polymerization of an Alkyne-Substituted N-carboxyanhydride and Click "Glycosylation. *Macromol. Rapid Commun.* **2010**, *31*, 991. (b) Cheng, Y. L.; He, C. L.; Xiao, C. S.; Ding, J. X.; Zhuang, X. L.; Chen, X. S. Versatile Synthesis of Temperature-Sensitive Polypeptides by Click Grafting of Oligo(Ethylene Glycol). *Polym. Chem.* **2011**, *2*, 2627. (c) Huang, Y. G.; Zeng, Y. H.; Yang, J. W.; Zeng, Z. H.; Zhu, F. M.; Chen, X. D. Facile Functionalization of Polypeptides by Thiol-Yne Photochemistry for Biomimetic Materials Synthesis. *Chem. Commun.* **2011**, *47*, 7509.
(29) Sánchez-Ferrer, A.; Mezzenga, R. Secondary Structure-Induced Micro- and Macrophase Separation in Rod-Coil Polypeptide Diblock, Triblock, and Star-Block Copolymers. *Macromolecules* **2010**, *43*, 1093.
(30) Venyaminov, S. Y.; Kalnin, N. N. Quantitative IR Spectrophotometry of Peptide Compounds in Water ($H_2O$) Solutions. II. Amide Absorption Bands of Polypeptides and Fibrous Proteins in Alpha-, Beta-, and Random Coil Conformations. *Biopolymers* **1990**, *30*, 1259. (b) Satoh, M.; Fujii, Y.; Kato, F.; Komiyama, J. Solvent- and Salt-Induced Coil−Helix Transition of Alkali Metal Salts of Poly(L-Glutamic Acid) in Aqueous Organic Solvents. *Biopolymers* **1991**, *31*, 1. (c) Ding, J. X.; Xiao, C. S.; Zhao, L.; Cheng, Y. L.; Ma, L. L.; Tang, Z. H.; Zhuang, X. L.; Chen, X. S. Poly(L-Glutamic Acid) Grafted with Oligo(2-(2-(2-Methoxyethoxy)Ethoxy)Ethyl Methacrylate): Thermal Phase Transition, Secondary Structure, and Self-Assembly. *J. Polym. Sci., Part A: Polym. Chem.* **2011**, *49*, 2665.
(31) Papadopoulos, P.; Floudas, G.; Klok, H. A.; Schnell, I.; Pakula, T. Self-Assembly and Dynamics of Poly(γ-benzyl-L-glutamate) Peptides. *Biomacromolecules* **2004**, *5*, 81.
(32) Jeon, S.; Choo, J.; Sohn, D.; Lee, S. N. Hydrogen Bonding Effects on the Conformational Changes of Polyglutamates Containing Long Flexible Side Chains. *Polymer* **2001**, *42*, 9915.
(33) Auer, H. E.; Mcknight, R. P. Two Classes of Beta Pleated-Sheet Conformation in Poly(L-Tyrosine): A Model for Tertiary Structure in Native Proteins. *Biochemistry* **1978**, *17*, 2798.
(34) Shih, K. Y.; Hsiao, T. S.; Deng, S. L.; Hong, J. L. Water-Soluble Poly(γ-propargyl-L-glutamate) Containing Pendant Sulfonate Ions and Terminal Fluorophore: Aggregation-Enhanced Emission and Secondary Structure. *Macromolecules* **2014**, *47*, 4037.
(35) Kuo, S. W.; Lee, H. F.; Chang, F. C. Synthesis and Self-Assembly of Helical Polypeptide-Random Coil Amphiphilic Diblock Copolymer. *J. Polym. Sci., Part A: Polym. Chem.* **2008**, *46*, 3108.
(36) (a) Prins, L. J.; Reinhoudt, D. N.; Timmerman, P. Noncovalent Synthesis Using Hydrogen Bonding. *Angew. Chem., Int. Ed.* **2001**, *40*, 2382. (b) Broer, D. J.; Bastiaansen, C. M. W.; Debije, M. G.; Schenning, A. P. H. J. Functional Organic Materials Based on Polymerized Liquid-Crystal Monomers: Supramolecular Hydrogen-Bonded Systems. *Angew. Chem., Int. Ed.* **2012**, *51*, 7102. (c) Chu, Y. L.; Cheng, C. C.; Yen, Y. C.; Chang, F. C. A New Supramolecular Hole Injection/Transport Material on Conducting Polymer for Application in Light-Emitting Diodes. *Adv. Mater.* **2012**, *24*, 1894. (d) Leigh, D. A.; Robertson, C. C.; Slawin, A. M. Z.; Thomson, P. I. T. AAAA-DDDD Quadruple Hydrogen-Bond Arrays Featuring NH···N and CH···N Hydrogen Bonds. *J. Am. Chem. Soc.* **2013**, *135*, 9939.
(37) (a) Gellman, S. H.; Dado, G. P.; Liang, C. B.; Adams, B. R. Conformation-Directing Effects of a Single Intramolecular Amide-Amide Hydrogen Bond: Variable-Temperature NMR and IR Studies on a Homologous Diamide Series. *J. Am. Chem. Soc.* **1991**, *113*, 1164. (b) Fielding, L. Determination of Association Constants ($K_a$) from Solution NMR Data. *Tetrahedron* **2000**, *56*, 6151. (c) Mesplet, N.; Morin, P.; Ribet, J. P. Spectrofluorometric Study of Eflucimibe-γ-cyclodextrin Inclusion Complex. *Eur. J. Pharm. Biopharm.* **2005**, *59*, 523.
(38) (a) Zu, S. Z.; Zhou, D.; Han, B. H. Supramolecular Surface Modification and Dispersion Of Graphene in Water and Organic Solvents. *J. Nanosci. Nanotechnol.* **2013**, *13*, 946. (b) Pochorovski, I.; Wang, H. L.; Feldblyum, J. I.; Zhang, X. D.; Antaris, A. L.; Bao, Z. N. H-Bonded Supramolecular Polymer for the Selective Dispersion and Subsequent Release of Large-Diameter Semiconducting Single-Walled Carbon Nanotubes. *J. Am. Chem. Soc.* **2015**, *137*, 4328.
(39) Murakami, H.; Nomura, T.; Nakashima, N. Noncovalent Porphyrin-Functionalized Single-Walled Carbon Nanotubes in Solution and the Formation of Porphyrin−Nanotube Nanocomposites. *Chem. Phys. Lett.* **2003**, *378*, 481.
(40) (a) Bahr, J. L.; Mickelson, E. T.; Bronikowski, M. J.; Smalley, R. E.; Tour, J. M. Dissolution of Small Diameter Single-Wall Carbon Nanotubes in Organic Solvents? *Chem. Commun.* **2001**, 193. (b) Giordani, S.; Bergin, S. D.; Nicolosi, V.; Lebedkin, S.; Kappes, M. M.; Blau, W. J.; Coleman, J. N. Debundling of Single-Walled Nanotubes by Dilution: Observation of Large Populations of Individual Nanotubes in Amide Solvent Dispersions. *J. Phys. Chem. B* **2006**, *110*, 15708.
(41) Ausman, K. D.; Piner, R.; Lourie, O.; Ruoff, R. S. Organic Solvent Dispersions of Single-Walled Carbon Nanotubes: Toward Solutions of Pristine Nanotubes. *J. Phys. Chem. B* **2000**, *104*, 8911.
(42) Huang, Y. Y.; Terentjev, E. M. Dispersion of Carbon Nanotubes: Mixing, Sonication, Stabilization, and Composite Properties. *Polymers* **2012**, *4*, 275.


DOI: 10.1021/acs.macromol.6b01060
*Macromolecules* 2016, 49, 5374−5385